ARMY RESEARCH LABORATORY

Fabrication and Testing of Tapered Electro-spray Nozzles

by Brendan M. Hanrahan and C. Mike Waits

ARL-TR-6226 **September 2012**

NOTICES

Disclaimers

The findings in this report are not to be construed as an official Department of the Army position unless so designated by other authorized documents.

Citation of manufacturer's or trade names does not constitute an official endorsement or approval of the use thereof.

Destroy this report when it is no longer needed. Do not return it to the originator.

Army Research Laboratory
Adelphi, MD 20783-1197

ARL-TR-6226 **September 2012**

Fabrication and Testing of Tapered Electro-spray Nozzles

Brendan M. Hanrahan and C. Mike Waits
Sensors and Electron Devices Directorate, ARL

REPORT DOCUMENTATION PAGE

Form Approved
OMB No. 0704-0188

1. REPORT DATE *(DD-MM-YYYY)*	2. REPORT TYPE	3. DATES COVERED (From - To)
September 2012	Final	1 January 2011 to 6 September 2012

4. TITLE AND SUBTITLE
Fabrication and Testing of Tapered Electro-spray Nozzles

5a. CONTRACT NUMBER

5b. GRANT NUMBER

5c. PROGRAM ELEMENT NUMBER

6. AUTHOR(S)
Brendan M. Hanrahan and C. Mike Waits

5d. PROJECT NUMBER

5e. TASK NUMBER

5f. WORK UNIT NUMBER

7. PERFORMING ORGANIZATION NAME(S) AND ADDRESS(ES)
U.S. Army Research Laboratory
ATTN: RDRL-SED-E
2800 Powder Mill Road
Adelphi, MD 20783-1197

8. PERFORMING ORGANIZATION REPORT NUMBER
ARL-TR-6226

9. SPONSORING/MONITORING AGENCY NAME(S) AND ADDRESS(ES)

10. SPONSOR/MONITOR'S ACRONYM(S)

11. SPONSOR/MONITOR'S REPORT NUMBER(S)

12. DISTRIBUTION/AVAILABILITY STATEMENT
Approved for public release; distribution unlimited.

13. SUPPLEMENTARY NOTES

14. ABSTRACT
The U.S. Army is interested in compact fuel-to-electric power systems to provide portable power sources for Soldiers and unmanned aerial vehicles (UAVs). This work describes multiple methods aimed at creating microfabricated, tapered-tip, electro-spray (E-spray) nozzles for efficient fuel injection. It has been shown that E-spray scaling depends on a number of factors, including nozzle/emitter geometry. Use of the new tapered nozzle tip diameters of 18 μm compared to a previous minimum of 30 μm allowed for E-spray operation below 0.01 ml/h at 70 °C fuel pre-heat, which is a 25-fold decrease over the minimum of 0.25 ml/h possible with 90-μm-diameter, flat topped nozzles at 56 °C. A dense array of tapered nozzles could meet a minimum power requirement, while using very low flow rates per nozzle to obtain small combustor geometries.

15. SUBJECT TERMS
Electro-spray, combustion, microfabrication

16. SECURITY CLASSIFICATION OF:			17. LIMITATION OF ABSTRACT	18. NUMBER OF PAGES	19a. NAME OF RESPONSIBLE PERSON
a. REPORT	b. ABSTRACT	c. THIS PAGE			Brendan M. Hanrahan
Unclassified	Unclassified	Unclassified	UU	30	19b. TELEPHONE NUMBER (*Include area code*) (301) 394-1960

Contents

List of Figures

List of Tables

1. Introduction

The U.S. Army is interested in compact fuel-to-electric power systems to provide portable power sources for Soldiers and unmanned aerial vehicles (UAVs). These energy systems use high-energy density fuels, such as jet propellant #8 (JP-8), small-scale fuel injection mechanisms, combustion, and a thermal-to-electric energy conversion process (*1*). Optimization of the fuel injection mechanism can lead to better heat utilization, reduced system volume, and increased system power density.

There are a number of fuel injection mechanisms for small-scale systems including direct vaporization, high pressure atomization, and electro-spray atomization (E-spray). This report focuses on improvements made to the E-spray fuel injection methodology developed by Deng et al. and Waits et al. (*2, 3*). The E-spray fuel injection mechanism is shown schematically in figure 1.

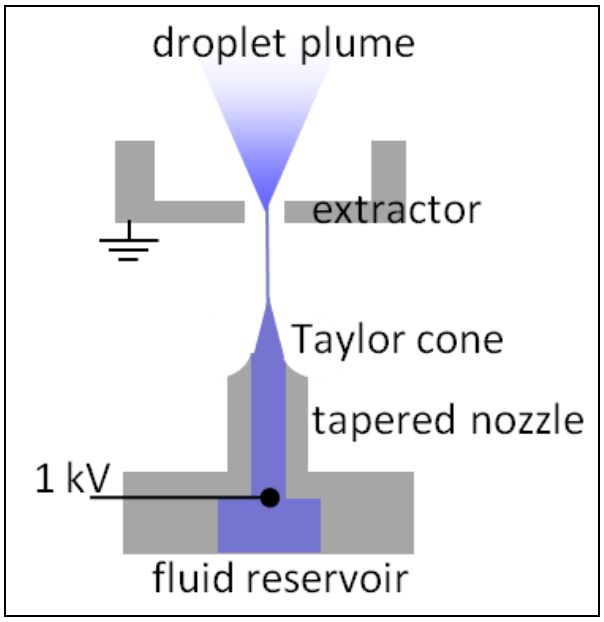

Figure 1. Schematic of a microfabricated E-spray fuel injection with tapered nozzle.

A high voltage is applied between the conductive liquid in the emitter nozzle and the extractor. The balance between the liquids capillary forces and the applied electric field form a Taylor-cone geometry at the tip of the emitter nozzle in the liquid, which subsequently emits a jet of liquid. The liquid jet periodically emits mono-dispersed diameter, charged liquid droplets through instabilities within the jet. Coulombic repulsion of the like-charged droplets accelerates them away from one another, creating a charged droplet plume.

The fundamental physics of E-spray have been described in a number of papers. Both Ganon-Calvo et al. and Fernández de la Mora derived power-law relationships between E-spray droplet size and liquid flow rate through the emitter, with lower flow rates giving significantly reduced droplet diameters (*4*, *5*). This power-law relationship for ethanol and JP-8 is shown in figure 2 for JP-8 and ethanol using a 1.63-mm outer diameter (OD) stainless steel tube. The droplet diameter was shown to scale with the flow rate (Q) to approximately the 0.5 power when spraying without an extractor. When spraying with an extractor, ethanol exhibit closer to 0.3 power, most likely due to the suppression of evaporation from the Taylor-cone. In order to preserve small droplet diameters at large flow rates, the fluid must be distributed through an array of nozzles (multiplexing).

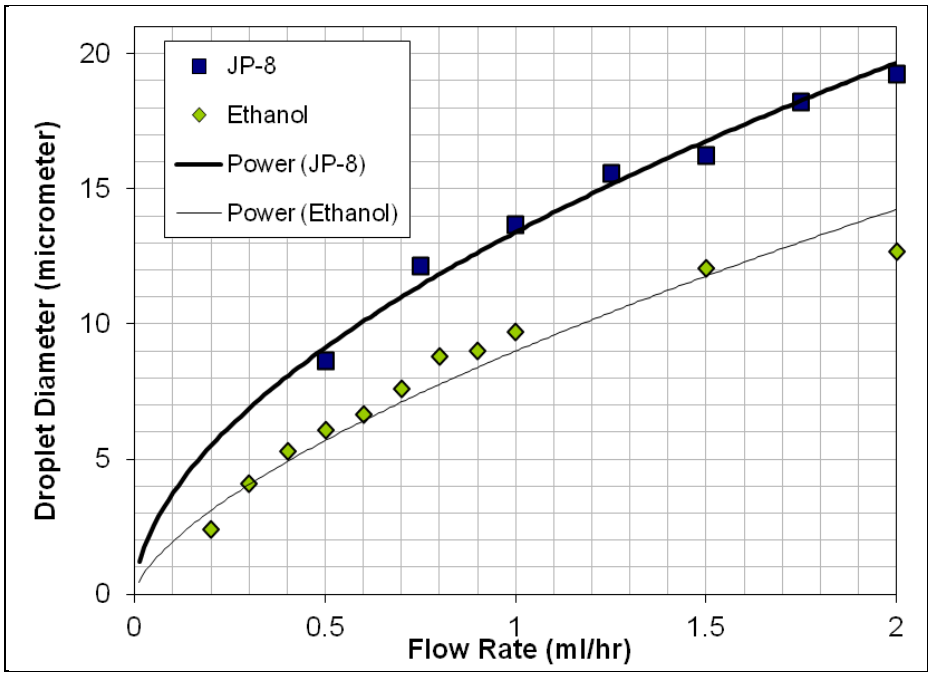

Figure 2. Droplet diameter variation with flow rate for JP-8 and ethanol.

To this end, a significant amount of work has been performed developing silicon-based, microfabricated E-spray systems for highly compact multiplexed electro-spray (MES). Silicon nozzles have been fabricated with outer diameters from 30 to 210 μm and extractor distances from 45 to 525 μm. High density microfabricated nozzle arrays have been demonstrated with greater than 11,500 nozzles/cm^2 (*2*), which have enabled liquid fluxes greater than 1 L/(h·cm^2) without an increase in droplet size. Additionally, multiple fuels have been sprayed through multiplexed nozzle systems, including ethanol, isobutanol, and JP-8.

Portable, compact, power generation systems place a high demand on volume optimization. To reduce the size of the fuel injection system, one should obtain the minimum evaporation distance for electro-sprayed droplets. Waits et al. derived the evaporation distance for a range of flow rates, finding that a minimum flow rate provided the smallest droplet size (*3*). Figure 3 was

generated using the D-square law of droplet evaporation and rates for ethanol evaporating within air at room temperature and for a range of droplet temperatures (*3*). Figure 3 demonstrates that extremely small droplet diameters or additional energy input to increase the droplet temperature are required to achieve evaporation lengths less than 1 mm. It is more beneficial to pursue techniques to reduce droplet diameters than to increase the energy input since this would be a loss in a power generation system. As seen from figure 3, the flow rate per nozzle must be minimized, for example, less than 0.05 mL/h to achieve a 1-μm ethanol droplet at room temperature.

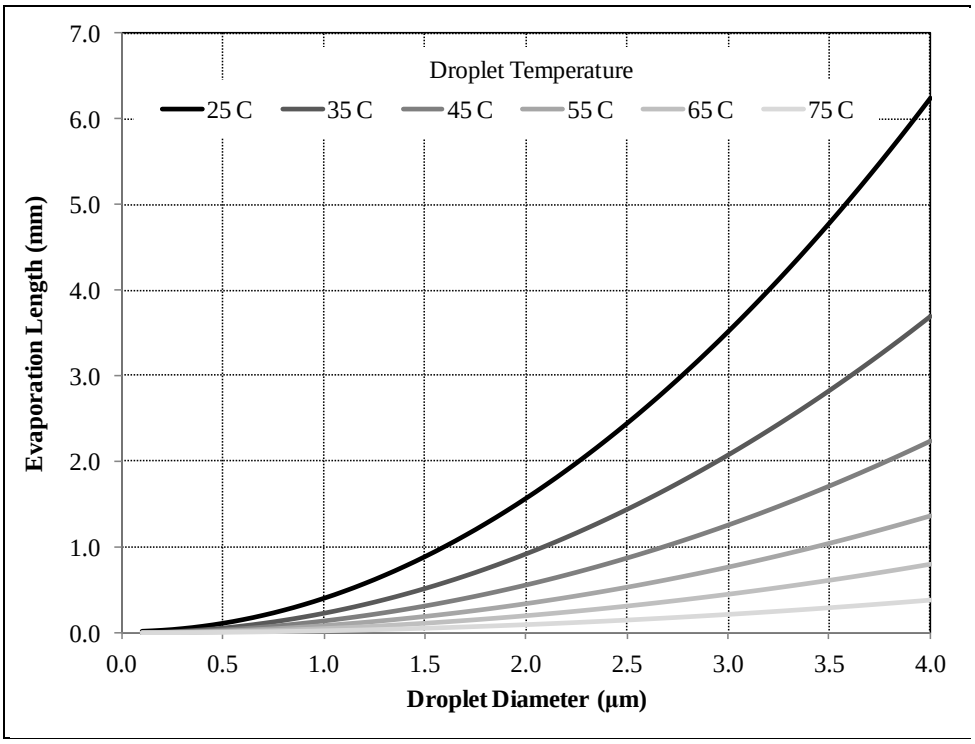

Figure 3. Evaporation length versus ethanol droplet diameter droplet temperatures ranging from room temperature to just below boiling and within air at room temperature.

The minimum flow rate is limited, by evaporation. In Deng's dissertation, he noted that the minimum flow rate in a microfabricated nozzle was determined by evaporation of liquid off the cone (*6*). When the evaporation rate is near the liquid flow rate, a stable Taylor-cone cannot be maintained which results in "dripping" or "spitting" mode. Thus, the minimum flow rate, and therefore the minimum droplet diameter, is determined by the nozzle's outer diameter. Langmuir derived an equation for evaporation rate (dM/dt), which depends on the difference in partial pressure of the vapor in the surrounding gas (Pp), the vapor pressure of the liquid (Pv), the mass of a molecule of liquid (m), temperature (T), and *k* is Boltzmann's constant.

$$\frac{dM}{dt} = (P_V - P_P)\sqrt{\frac{m}{2\pi kT}} \quad (1)$$

The Langmuir equation represents an evaporation rate per unit area, thus evaporation scales linearly with the exposed area or OD of the nozzle.

Deng et al. have also demonstrated a faster response time with a reduction in the outer nozzle diameter, which is beneficial for reciprocating engines. In the same paper, Deng et al. found that the mass of fluid in the Taylor-cone, conductivity, and liquid viscosity affected the spray turn-on time (*7*). The mass of the fluid can be controlled by the nozzle outer diameter, which determines the size of the Taylor-cone. He demonstrated a reduction in the response time with the outer diameter, stating that 60 μm, showing a response time of 150 μs, was the practical limit due to the current state-of-the art fabrication techniques using strictly vertical silicon nozzles.

In addition to shorter evaporation lengths and faster response times, the on-set voltage to form a Taylor-cone reduces with a decreased outer nozzle diameter. Krpoun et al. and Velásquez-García et al. both suggest the cone formation voltage scales logarithmically with the outer nozzle diameter for diameters relevant to microfabricated nozzles (*8*, *9*). Figure 4 shows the approximate cone formation voltage versus the nozzle OD for the relationships provided by Krpoun et al. and Velásquez-García et al.

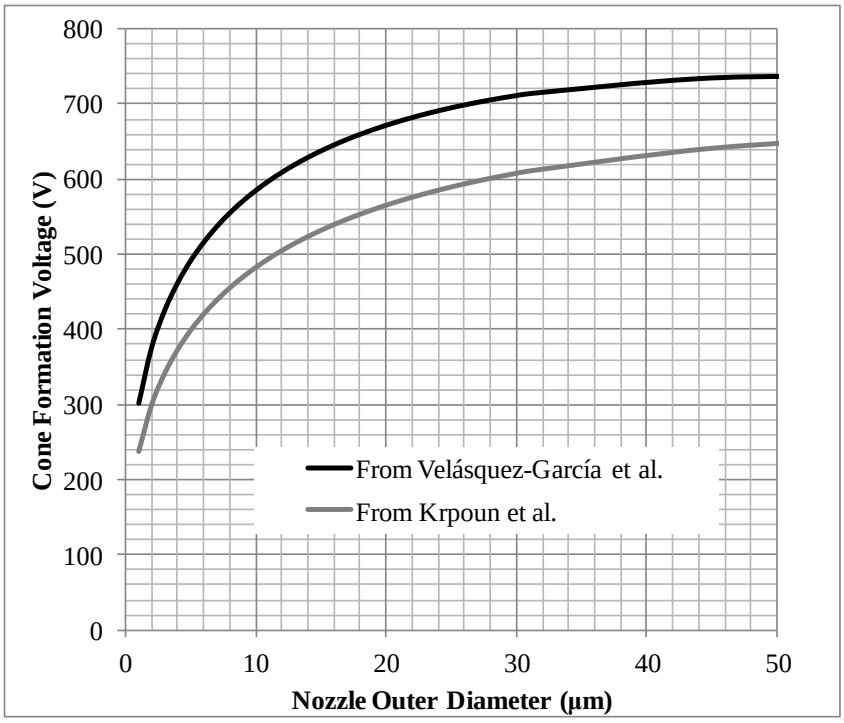

Figure 4. Minimum voltage to form a Taylor-cone versus the OD of the nozzle using the relationships developed by Krpoun et al. and Velásquez-García et al. (*8*, *9*).

The nozzle OD is the critical parameter when scaling E-spray devices as it determines a number of performance metrics like the evaporation length, response time, and cone formation voltage. This work describes the custom fabrication of microfabricated E-spray nozzles to reduce the

nozzle OD below the current limitations of vertical wall nozzles by tapering the nozzle tip, as described by Deng et al. (*2*). Furthermore, we report a significantly reduced flow rate operation versus macroscale and previously microfabricated emitters.

2. Fabrication

The microfabricated E-spray described here is composed of three layers: (1) an extractor layer, (2) a nozzle layer, and (3) a NanoPort™ adapter with a stainless steel tubulation. The extractor layer is fabricated in a 200-µm-thick, double-side-polished silicon wafer, and is aligned to the nozzle layer to form an MES device through a previously described method using optical fibers of a known diameter (250 µm) (*2*, *3*). The MES device is then assembled with fluidic connections as shown in figure 5. The NanoPort™ and stainless steel tabulation is described in detail in section 3. The focus of this report is on the nozzle layer, specifically the custom fabrication scheme to minimize the outer diameter.

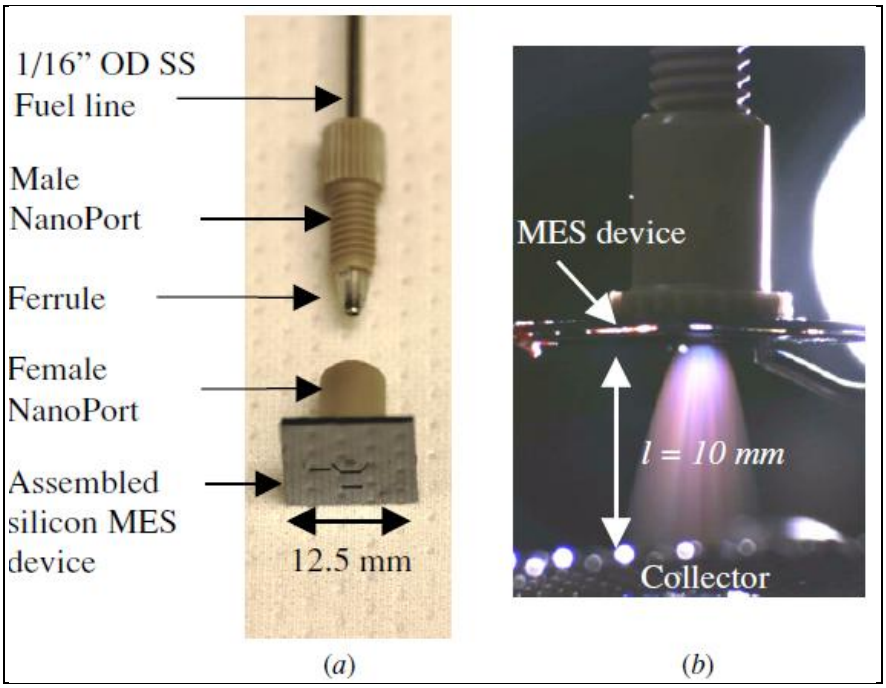

Figure 5. (a) Photograph of MES assembly components and (b) photograph of an operating MES device.

Microfabrication is a core technology allowing the realization of small features close-tolerance structures. One of the limitations of microfabrication is the ability to make sloping structures. This work describes three different methods investigated to obtain tapered nozzle tips compared to the flat-top microfabricated nozzles previously described. Figure 6 compares the geometry of flat top (figure 6a) and tapered nozzles (figure 6b).

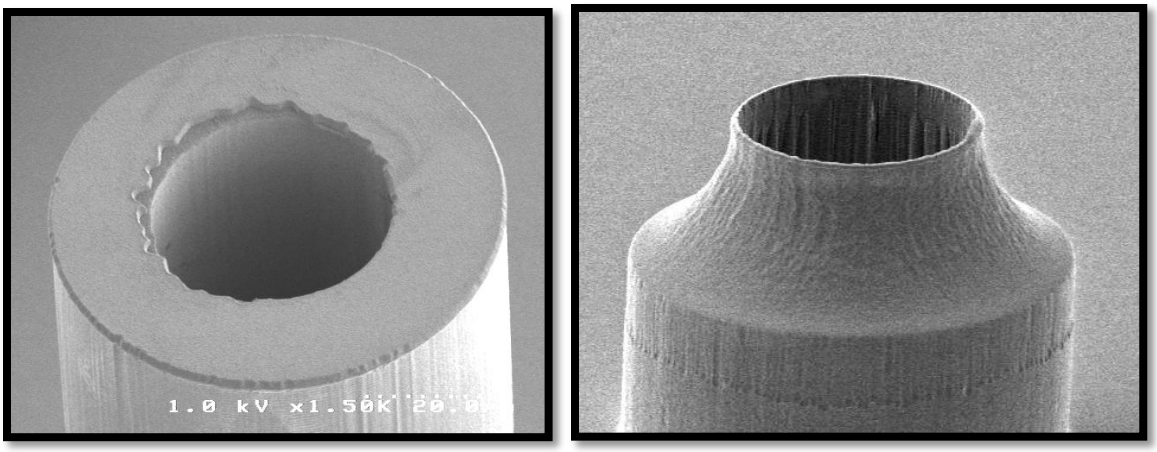

Figure 6. (left) Flat-top nozzle tip and (right) isotropically etched tapered nozzle tip.

The structural integrity of the nozzle is determined by the material thickness between the internal through hole and OD of the nozzle. It was previously determined that 60 μm was the minimum OD possible for the flat top nozzle, primarily due to a necking of the nozzle towards the base weakening the nozzle (*7*). The tapered nozzle design effectively uses the inner diameter (ID) as the outer diameter, and therefore the base diameter can be significantly larger than the ID while still maintaining the desired small Taylor-cone radius.

2.1 Extractor Fabrication

The extractor fabrication uses successive deep-reactive ion etch (DRIE) steps. This process is only briefly described below. For a more thorough explanation, please reference the work by Deng et al. (*10*). The extractor is fabricated in two etch steps. The first etch defines the hole for the spray to pass through as well as the alignment trenches. The alignment trenches have specific depth requirement of >150 μm. The extractor wafer is then flipped over, and an etch is performed on the opposite side of the wafer defining a cavity. The depth of this etch is determined by the difference in the wafer thickness and the depth of the front-side etch. A cross section of the extractor layer is provided in figure 7.

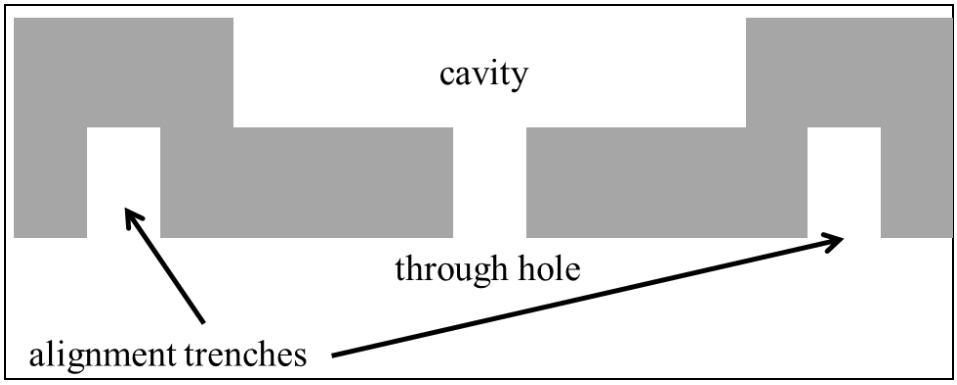

Figure 7. Cross-sectional schematic of extractor layer.

2.2 "Top Hat" Fabrication Method

The goal of this fabrication method was to create the tapered nozzle geometry using only plasma-based etching. The advantages of using plasma-only processes are better across-wafer uniformity, easier process control, and fewer challenges with etch rate selectivity between materials when compared to the alternative wet etch processes using chemicals such as hydrofluoric acid + nitric acid + acetic acid (HNA). Tight control of bath temperatures and agitation are difficult and often result in poorer uniformity etches when compared to plasma processes.

A process flow is provided in figure 8. The first steps in the process deal with defining the inner and outer nozzle diameters. The first step in the process was to deposit 3 µm of silicon dioxide (SiO_2) on the topside of a 500-µm-thick, double-side-polished silicon wafer. Contact photolithography is performed to define the nozzle outer diameter. A methane (CH_3) plasma based etch is used to completely etch the SiO_2 not protected by photoresist at a rate of 6 min/µm (figure 8b). Contact photolithography was then performed to define the nozzle ID on top of the remaining SiO_2 after the previous etch. The exposed oxide is only partially etched (2 µm) such that a 3-µm-thick SiO_2 layer defines the outer nozzle base and a 1-µm-thick SiO_2 defines the nozzle ID (figure 8c). This multi-level oxide process will serve as a hardmask for future etching.

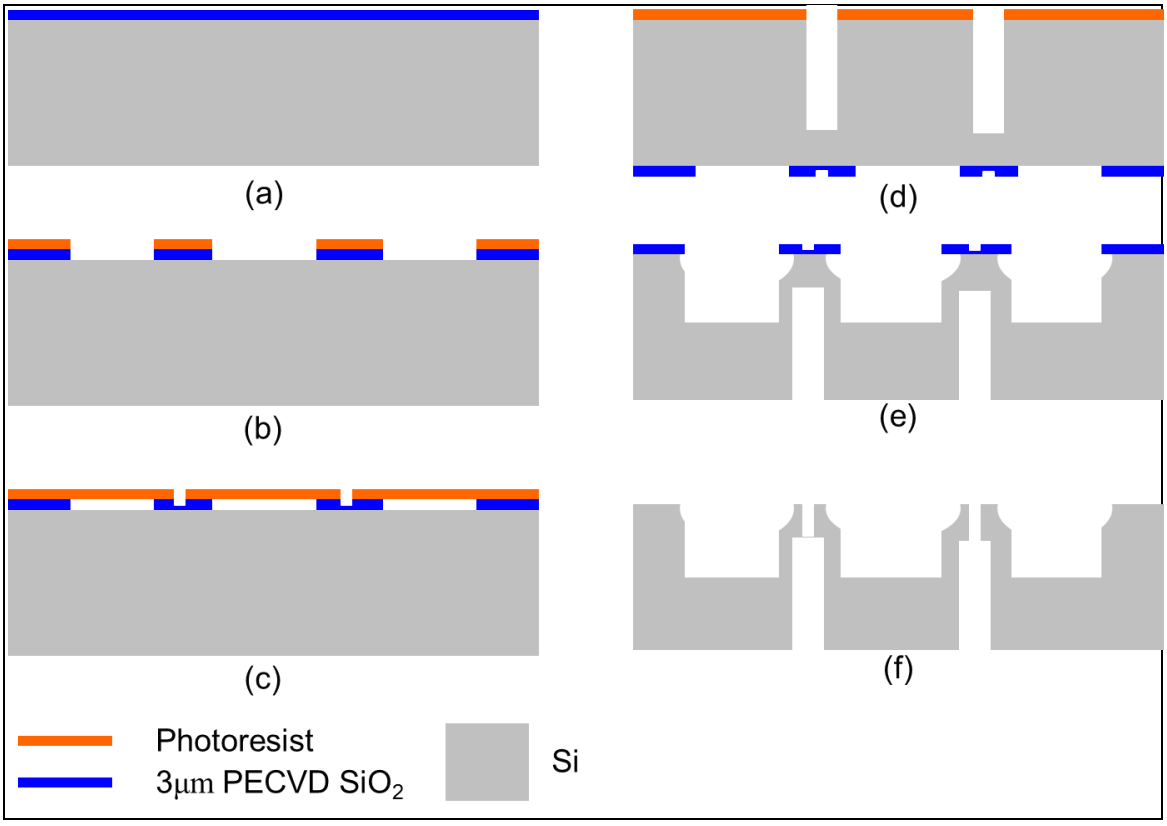

Figure 8. Process flow for "Top Hat" tapered nozzles.

Once the multi-thickness nozzle hardmask is defined in the oxide, the wafer is turned-over for further processing. Contact photolithography is performed on the backside of the wafer, used to define the backside through-hole, which has a diameter in-between the inner and outer diameters. The nozzle cross section is shown in figure 9. The backside etch, performed using DRIE was designed to be a depth that would extend through the wafer, halfway into the nozzle height (figure 8d). One of the challenges of this etch is that it is difficult to measure the etch depth of high aspect-ratio structures because it is difficult to see reflected light in them. Therefore, the etch rate and depth could only be estimated from early measured values before the hole became too deep.

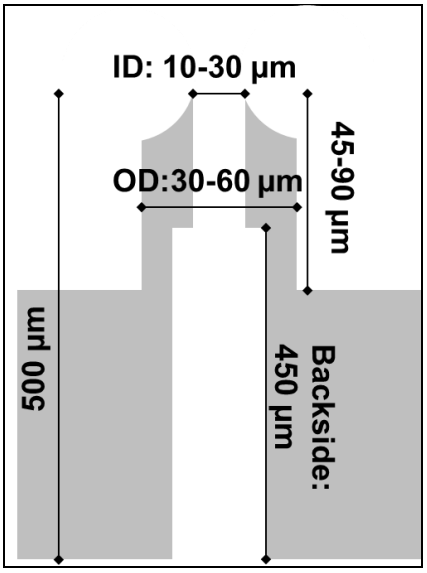

Figure 9. Dimensioned nozzle showing range of possible dimensions.

Upon completion of the backside etch, processing was continued on the front-side of the wafer. The next etching step defines the taper of the nozzle. The nozzle tapering etch is done by using an isotropic, sulfur hexafluoride (SF_6) plasma-based process (figure 8e). The parameters for the etch process are listed in table 1.

Table 1. Isotropic etch parameters.

Plate power (W)	Chamber pressure (mTorr)	RF coil power (W)	Plate temp (°C)	SF_6 flow (sccm)	Ar flow (sccm)
10	22	850	30	100	40

The etch process parameters were tuned to provide consistent properties like etch depth and etch profile. The lateral etch rate is measured via optical microscopy. The etch front can be observed beneath the semi-transparent SiO_2 thin film. When the isotropic etch was within 2–5 µm of the nozzle ID, the isotropic etch was considered completed, leaving a top hat of oxide film suspended above the tapered nozzle.

At this point, the multi-level oxide mask had thinned slightly but was nearly at the original 3 μm/1 μm for the OD, and ID thicknesses respectively as before. The ID oxide was then removed by a 6-min blanket CH_3 plasma etch, leaving only a ring of suspended oxide film remaining and thinning the 3-μm film to less than 2 μm. The next etch step used DRIE to etch both the nozzle OD and ID (figure 8f), with the goal of defining an appropriately tall nozzle while reaching the backside through hole with the ID etch (refer to figure 9).

There were a number of issues with this process design. These issues included insufficient backside etch depths, tapering of nozzle OD towards reduced diameter during the nozzle etch, and over-etching of the isotropic, nozzle tapering etch.

The backside through hole etch is performed using a photoresist mask and DRIE. The selectivity of photoresist to silicon etch rate in DRIE is 1:100–150; therefore, a 10-μm photoresist mask should be sufficient to mask up to 1 mm of silicon etching ideally. The silicon etch rate, however, becomes aspect ratio and etch depth dependent in narrower/deeper structures. The hole diameters were 15–45 μm, which gives aspect ratios of nearly 1:33 and 1:10. The former is at the limits of even advanced DRIE tools and the latter requires tailoring of the DRIE process for the Versalock™ DRIE tool available. This resulted in a rapidly decelerating etch rate and tapering of the backside hole diameter due to the inability for reactive species to reach the bottom of the etched feature. The challenge described earlier is that it is difficult to measure the depth of deep-etched holes. Initial etch rates were taken on 50-μm-diameter holes and found to be <2 μm/min after 60 min of etching, which is significantly slower than the usual <3 μm/min observed in the Versalock™ DRIE tool. As this etch is continued, the etch rate of silicon continues to slow down, and it was found that we could not obtain the desired backside etch depths. Eventually the etch mask fails before the silicon reaches the appropriate depth. For future attempts at such a process, we suggest changing the chamber power and gas pressure to try and obtain more directional, deeper-etching ions.

The second issue was the tapering of the nozzle outer diameter. An example of this is shown in figure 10.

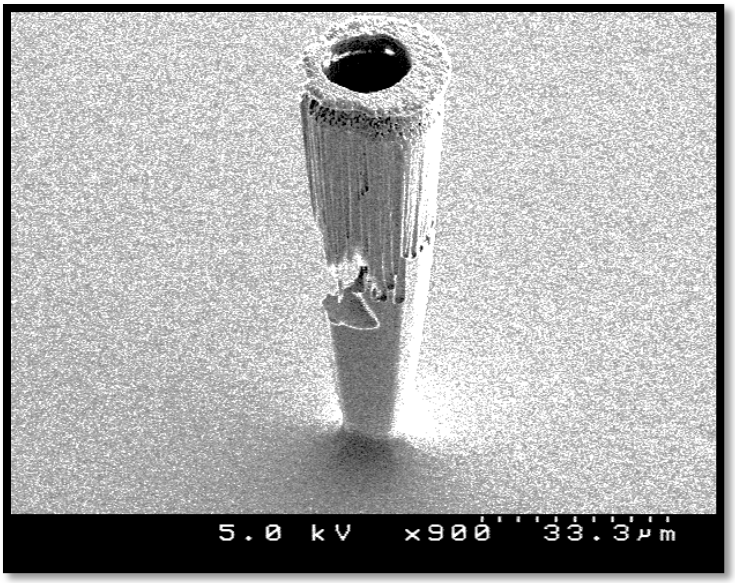

Figure 10. SEM image of severely tapered nozzle OD etch.

Figure 10 shows a nozzle with severe tapering. The nozzle ID has come into contact with the outer wall, rendering the nozzle useless. The recipe was then tuned to reduce the nozzle taper by changing the plasma pressure. Figure 11 shows a nozzle using the tailored "no-lag" DRIE recipe.

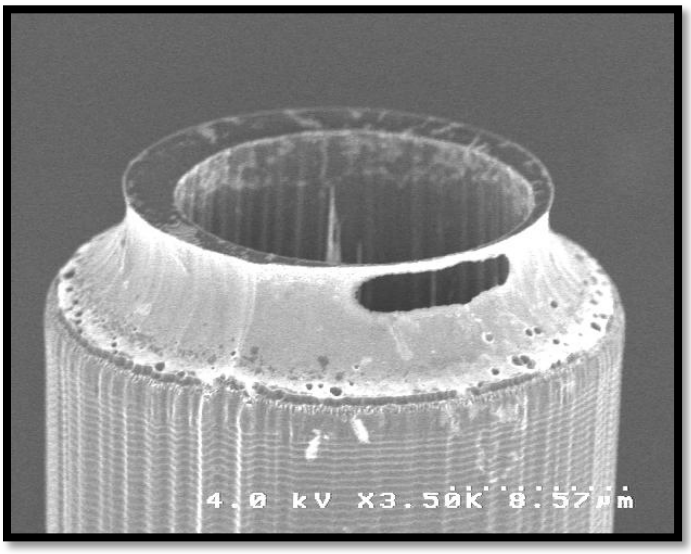

Figure 11. Scanning electron microscopy (SEM) image of isotropic over-etch apparent on nozzle tip.

Nozzle OD taper was reduced in this case and this SEM image also highlights the third issue with the "top hat" etching process, which is due to over-etching if the isotropic etch process or misalignment of the nozzle ID. This issue is shown schematically in figure 12.

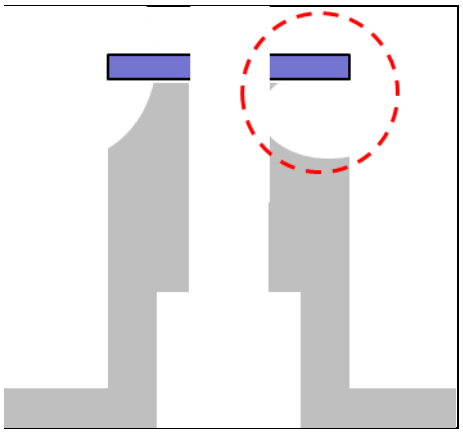

Figure 12. Schematic of isotropic over-etch.

The isotropic over-etch/misalignment can result in a hanging OD etch mask, which has the potential of breaking off. The breaking through of the isotropic etch will also result in unusable nozzle. To solve this problem, careful care must be taken with the alignment and the isotropic etch cannot be too aggressive geometrically, i.e., within 3 µm of the nozzle's ID.

Ultimately, these challenges prevented a working prototype from being realized. Therefore, a new fabrication process was proposed to try and obtain deeper backside etching and better alignment.

2.3 Thermal Oxidation Method

Upon the failure of the "top hat" method, a new approach was taken to assure that the nozzle ID and backside etch made contact for a continuous fluid channel. The next nozzle fabrication method depends significantly upon a thermal oxidation of the etched tapered nozzle. A fabrication process schematic is shown in figure 13.

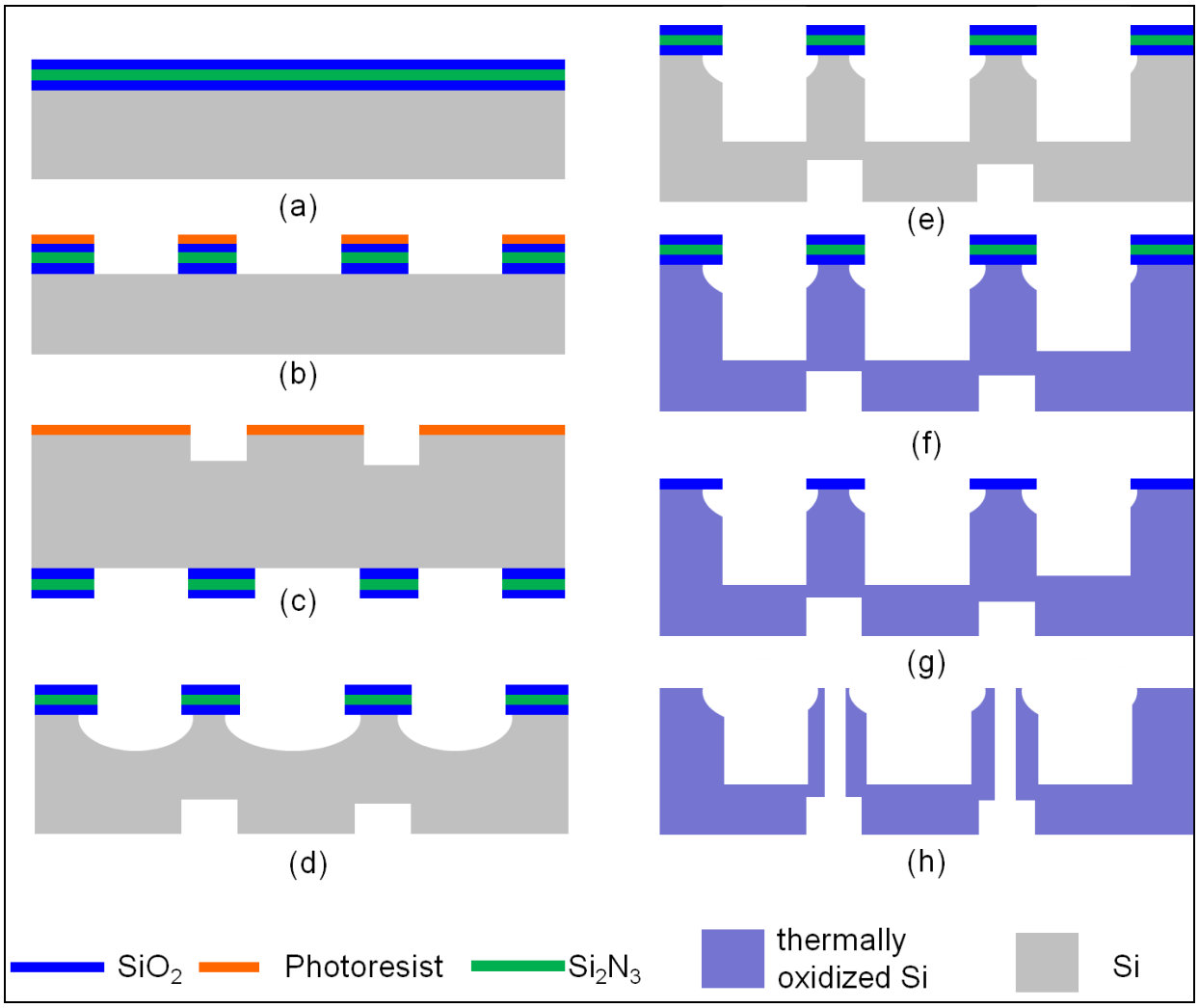

Figure 13. Fabrication process for thermally oxidized isotropic nozzles.

The first step in this process was to deposit and pattern a three-layer stack of SiO_2/silicon nitride (Si_2N_3)/SiO_2 (figure 13a and b). The first SiO_2 layer was used to help balance the film stress and was 100 nm thick. The second layer, 100-nm-thick silicon nitride, was used for a sacrificial etch later on in the process. The third and final layer was a 1–3 µm thick silicon dioxide layer, which is used as the nozzle OD mask as is the case with the previously described "top hat" process. The next step is the backside DRIE to define the backside holes (figure 13c).

After the backside holes are etched, the three layer stack serves as the mask for the isotropic nozzle etch (figure 13d). The most important feature of this etch is the lateral etch distance, which will ultimately define the nozzle ID. The lateral etch rate is determined via optical inspection of the diameter of a visible color change in etch mask, as shown is figure 14 with a progression of three etches.

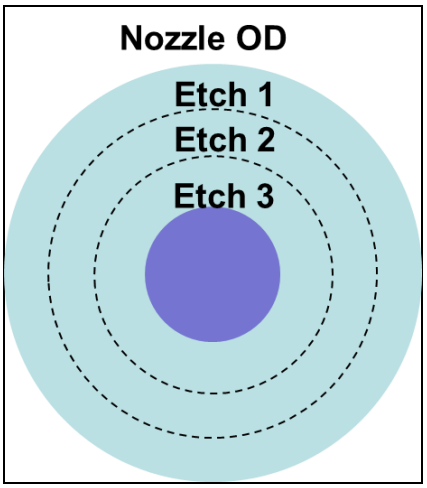

Figure 14. Top-view of tapered nozzle through progressive isotropic etching times.

Once the isotropic etch has reached a diameter of 10–15 μm, the process is stopped. The next step (figure 13e) uses the floating three-layer stack as an etch mask to define the height of the nozzle. The nozzle height is etched out of silicon using tuned no-lag DRIE recipe, described in section 1.2.

The next step is a series of wafer cleaning steps and thermal oxidation (figure 13f). The process is called the RCA clean, named after the Radio Corporation of America. The first bath, RCA1, is performed using a 1:1:5 solution of ammonium hydroxide (NH_4OH) + hydrogen peroxide (H_2O_2) + water (H_2O) heated to 80 °C. This step removes organic materials. The second step is a heated solution, 1:1:6 of hydrogen chloride (HCl) + H_2O_2 + H_2O to remove traces of metal ions, which could contaminate the thermal oxidation furnace.

Thermal oxidation takes place by providing the oxidant, either O_2 or H_2O, energy in the form of high heat, and silicon on the wafer, which gets gradually consumed. If the nozzle ID was too small, from the isotropic etch becoming too aggressive, the whole nozzle tip could be oxidized, removing the etch mask, as shown in figure 15.

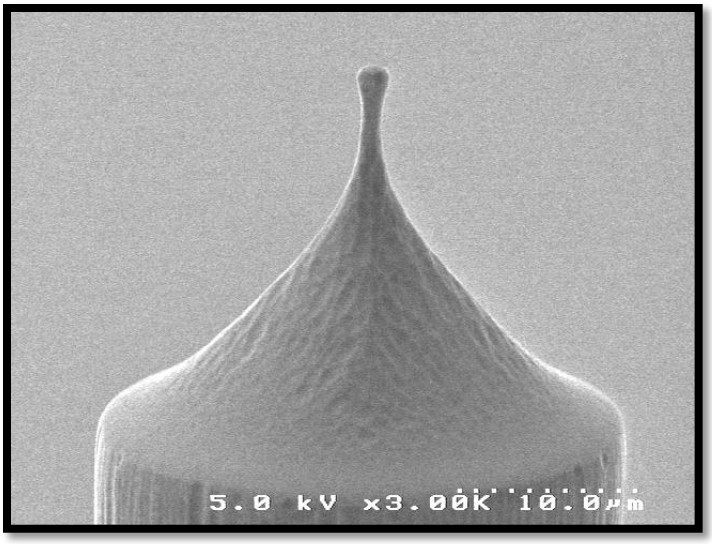

Figure 15. Over-etched nozzle OD after thermal oxidation.

The nozzles that were not over-etched were next placed in a hot phosphoric acid etch bath at 160 °C, which was meant to selectively etch the Si_2N_3 layer, thereby removing the floating etch mask (figure 13g). The etch rate of Si_2N_3 was reported to be 20 nm/min, compared to 0.18 nm/min for thermal oxidation-derived SiO_2 (*11*). It was found that despite the two orders of magnitude difference in etch rate, the acid etch had a difficult time reaching the Si_2N_3 interlayer, so etch times were significantly longer than expected. One wafer had the thermal oxide layer completely destroyed before the interlayer was removed after 4 h of etching.

The cap was attempted to be removed using mechanical vibration provided ultrasonically before the acid etch step. An SEM image of a broken cap is shown in figure 16.

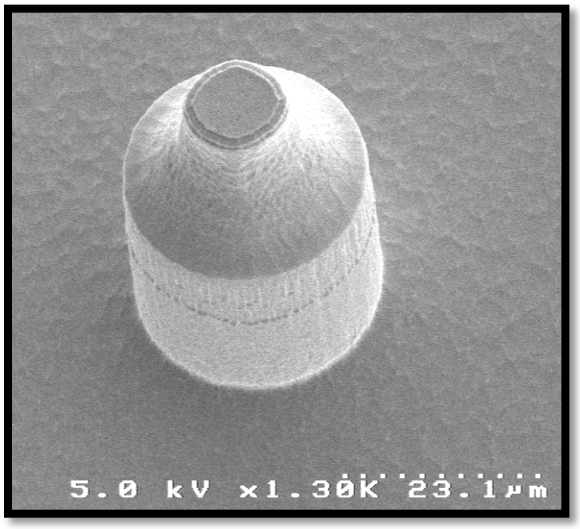

Figure 16. SEM image of thermally oxidized nozzle with broken top cap.

The ultrasonic breaking of the etch mask was found to be a low-yield methodology, with some caps breaking and others folding and sticking to the side of the nozzle.

Ultimately, this method was abandoned due to difficulties in removing the nozzle OD layers to continue the fabrication process. If materials could be used with thicker layers and higher selectivities, then we believe this would be a reliable process to obtain microfabricated tapered nozzles.

2.4 Inner Diameter Pre-etch Method

The main issue with the "top hat" method was the inability to have the nozzle ID etched hole reach the backside etched hole to make a continuous flow path. To solve this problem, a fabrication scheme was developed that focused on reaching the intended ID depth early on in the process. The ID pre-etch process described in this section was also the shortest and simplest. This process flow is shown in figure 17.

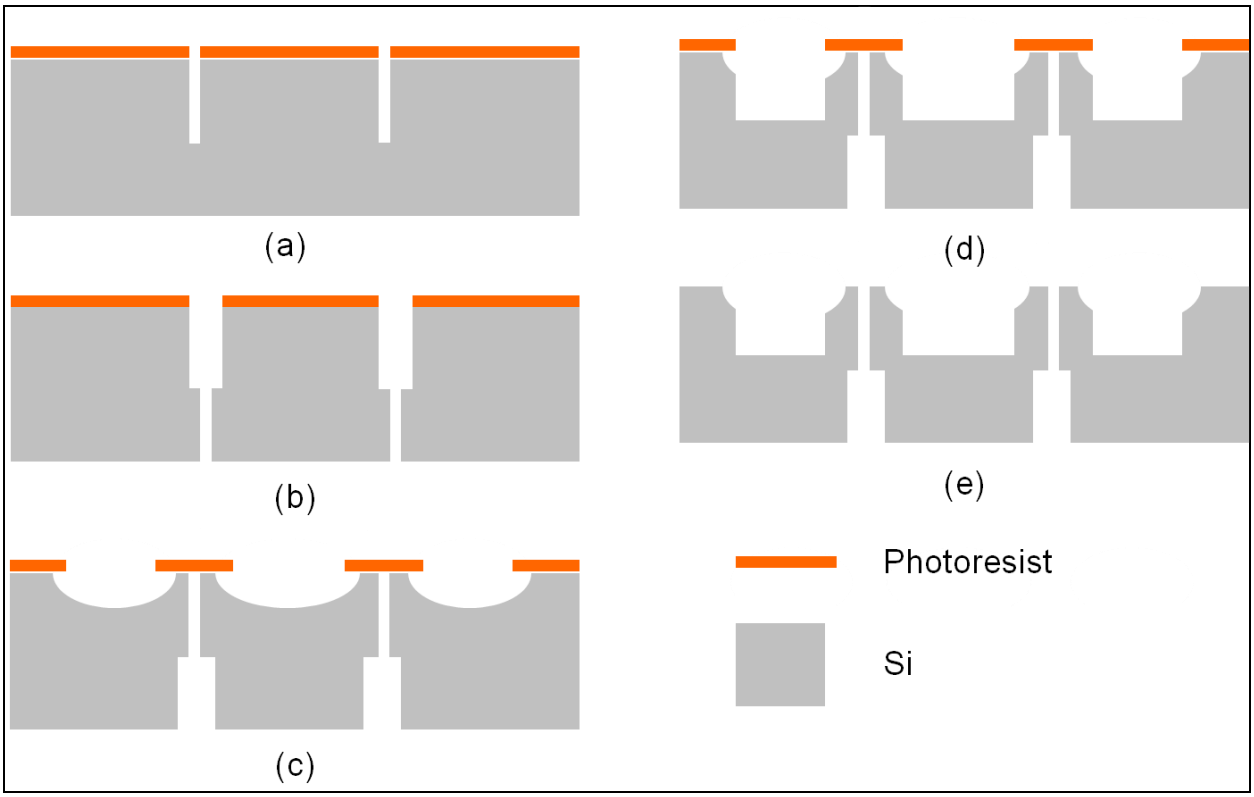

Figure 17. Fabrication process flow for the ID pre-etch method.

The first step in this process is to define the nozzle ID with contact photolithography and a DRIE process (figure 17a). This etch was performed for 150 min and the depth was unmeasureable, but assumed to be greater than 200 μm. The next step (figure 17b) was the aligned backside through holes, defined using contact photolithography and DRIE. This etch was performed until the ID

hole was visible at the bottom of the backside hole, thereby guaranteeing a through-hole had been created.

Once the through-hole had been created, the rest of the nozzle needed to be defined. To do this, thick AZ 9245™ photoresist was spun at 500 rpm for 10 s and then 1000 rpm for 30 s. This allowed the photoresist to maintain its integrity while spanning the nozzle ID holes. Contact photolithography was performed to define the nozzle OD. The next two steps were the isotropic nozzle etch (figure 17c) and no-lag DRIE (figure 17d) to define the nozzle taper and height, respectively. These etches were performed in the manner described in the previous two sections. Finally, the device was cleaned (figure 17e) removing the remaining photoresist and diced, resulting in the first successful microfabricated tapered nozzles. Nozzles with 45 μm OD/18 μm ID (figure 18) and 60 μm OD/36 μm ID were obtained.

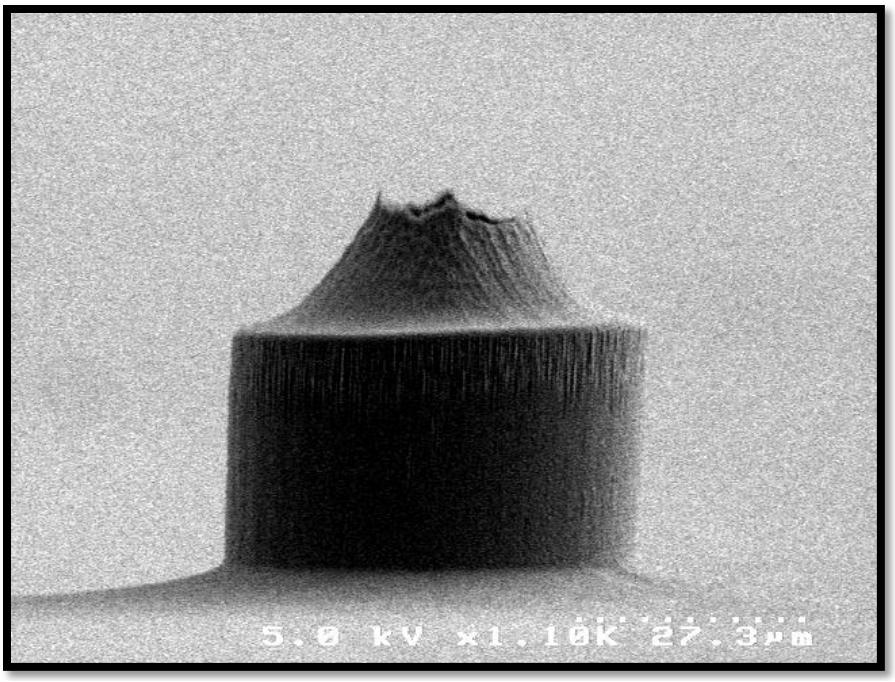

Figure 18. SEM image of completed tapered nozzle.

The tip of the smallest tapered typically showed a jagged edge after cleaning due to a crack induced from an isotropic over etch similar to the one shown in figure 11.

3. Experimental Methods

The purpose of the tapered nozzle was to allow for the lowest flow rate per nozzle possible, while maintaining the structural integrity of the nozzle. The low flow rate operation of the tapered nozzle produces small droplets, which are evaporated in small distances, enabling

smaller systems. The tapered nozzle also emits a smaller Taylor-cone, which can help increase the transient response of the nozzle and reduce the voltage required to form the Taylor-cone.

The goal of the experiments was to determine the minimum flow rate for three nozzle varieties: a stainless steel tubulation of 1.63 mm diameter, a flat-topped microfabricated nozzle with 90 μm OD as described in Deng et al., and a tapered nozzle of 18 μm. A photograph of the nozzle testing setup is shown in figure 19. A visual inspection method was used to determine the E-spray operating regime to determine minimum flow rate. A collimated light source combined with a long working distance (WD) microscope lens allowed for 1-μm/pixel camera resolution. Various levels of fuel pre-heat were introduced through resistive heating tape applied to the stainless steel fuel line. Fuel was pumped using a computer controlled gear pump (M6 Vici™ liquid handling pump).

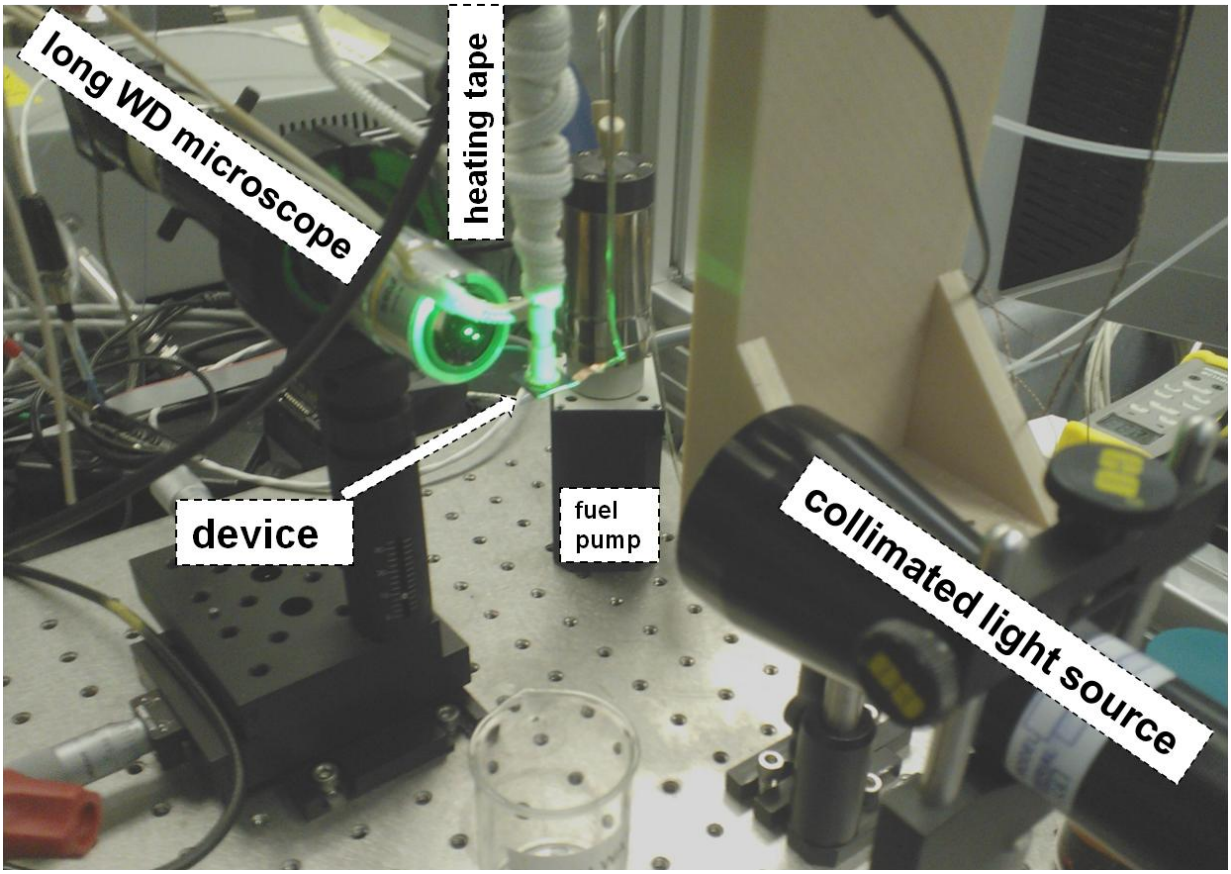

Figure 19. Photograph of experimental setup.

The device hung beneath a custom fabricated arm allowing for intimate, large area contact between the heating tape and fuel input line to assure isothermic conditions. Temperature was measured via thermocouples imbedded within the heating tape wrap. The device was epoxied to a plastic ferrule in a manner described by Waits et al. (*3*).

Testing was performed by monitoring the electro-sprayed ethanol visually. Ethanol was chosen for this test due to its high vapor pressure and conductivity. If evaporation dominated the low flow rate operation of E-spray nozzles, then the effect would be better observed using high vapor-pressure, fast evaporating fluids. Additionally, the fluid must have some conductivity in order to be manipulated by an electric field.

Experiments were done by progressively heating the fuel and observing changes in the E-spray characteristics. Fuel temperature was given 10 min to equilibrate in between temperature changes, and a fuel was considered to be at its minimum flow rate when it displayed consistent operation for over 5 min. An example image of a microfabricated flat-top nozzle spraying is shown in figure 20.

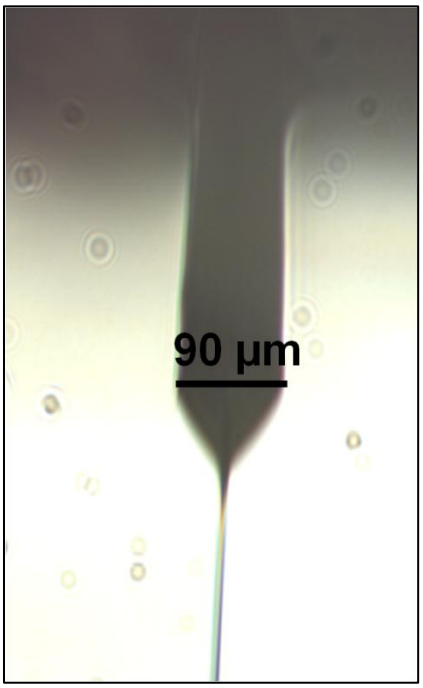

Figure 20. Photograph of flat top nozzle in operation.

As a point of comparison, an image of a spraying tapered nozzle is shown in figure 21.

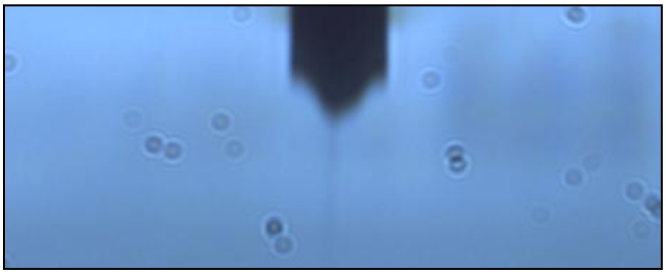

Figure 21. Photograph of tapered nozzle in operation.

The very low flow rates obtained with tapered nozzle became increasingly difficult to observe, so the observation of a jet was used a confirmation of stable E-spray.

4. Results and Discussion

4.1 Minimum Flow Rate vs. Temperature

The main goal of this experiment was to establish a minimum flow rate for different diameter E-spray nozzles, over a range of temperatures. Given that minimum flow rate is evaporation dependent; the smallest diameter nozzle should have the smallest evaporation rate due to reduced fluid area. The minimum observed flow rate for the three nozzle variations is shown in figure 22 for a range of fuel temperatures below the boiling point of ethanol.

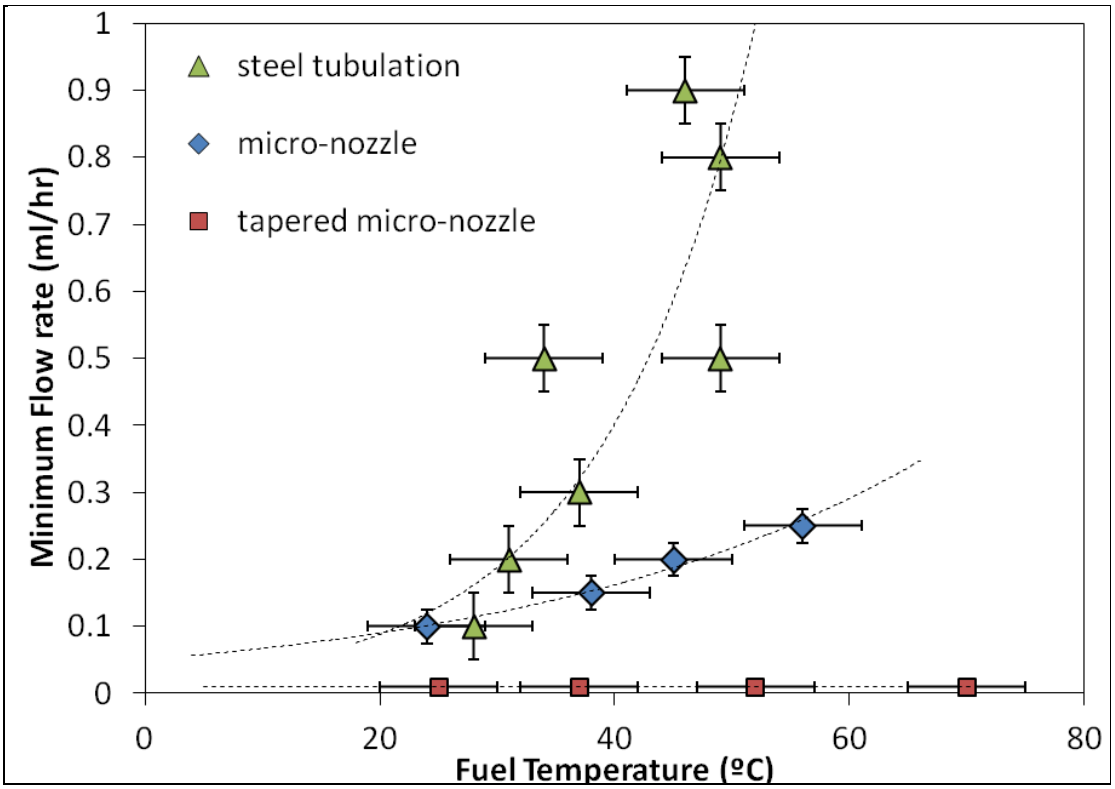

Figure 22. Comparison of minimum flow rate amongst three nozzle varieties: stainless steel tabulation, 90-µm-OD flat-top nozzle, and 18-µm-OD tapered nozzle, over a range of fuel temperatures.

Figure 22 shows that over the range of temperatures tested, a minimum flow rate was not observed for the tapered nozzle, but rather the nozzle was able to operate at the lower limit of the pump. The tapered nozzle operated at low enough flow rates that electrohydrodynamic pumping was possible, i.e., the electric field pulled the fluid from the emitter at very low >0.005 ml/h flow rates suggesting droplet diameters well below 0.5 µm are possible.

These results show the potential of the nozzle tapering process. The tapered nozzle process was performed on single nozzle devices, but it was designed to be compatible with multiplexed nozzle arrays. A dense array of tapered nozzles could meet a minimum power requirement, while using very low flow rates per nozzle to obtain small combustor geometries.

4.2 Microclimate

One of the challenges with this experiment is assuring the experimental conditions are consistent among devices. The microfabricated nozzles had the unique condition created by having a nearly closed volume around the nozzle, created by the extractor chip. The conditions of this closed volume could affect the evaporation rate of fuel off the Taylor-cone.

To determine if there is an influence of microclimate, the evaporation rate was calculated from the Langmuir equation 1, using the fluid vapor-pressure and the surface area of the Taylor-cone for each nozzle geometry. The 90-μm-diameter nozzle has a Taylor-cone surface area of 1.422×10^{-8} m^2 and a calculated liquid evaporation rate ranging from 9.7 to 98 nL/h for liquid temperatures from 26–77 °C. The 18-μm-diameter tapered nozzle has a Taylor-cone surface area of 5.69×10^{-10} m^2 and a calculated liquid evaporation rate ranging from 0.4 to 4 nL/h for liquid temperatures from 26–77 °C. The expansion ratio of ethanol (density of gas/density of liquid) is 420 and the volume of the extractor chamber is estimated to be 2×10^{-8} m^3. Given the evaporation rate, expansion ratio, and open volume, and assuming no vapor is removed from the chamber, it would require a minimum of 12 and 0.5 h to saturate the environment for the 18-and 90-μm nozzles, respectively. These timescales suggest that microclimate creation was not an issue during our experiments and the benefit of scaling nozzle diameter observed was minimally influence by microclimate evaporation retardation. Future work on multiplexed devices will investigate the increased cone evaporation area from using multiple nozzles and the ability to reach a saturation condition more quickly. Extremely low flow rates, and thus small droplet diameters and evaporation distances, should be achievable through the combination of multiple nozzles, an extractor design that minimizes vapor loss, and the tapered nozzle tips presented here.

5. Summary and Conclusion

This work has described multiple methods aimed at creating microfabricated, tapered-tip, E-spray nozzles. The U.S. Army desires compact liquid fuel-to-electric power systems, and part of such a system would be a fuel injector. E-spray has been explored for fuel injection as it is a low power, compact mechanism. It has been shown that E-spray scaling depends on a number of factors, including nozzle/emitter geometry. Tapered nozzle tip diameters of 18 μm compared to a previous minimum of 30 μm has allowed for E-spray operation below 0.01 ml/h at 70 °C fuel pre-heat, which is a 25-fold decrease over the minimum of 0.25 ml/h possible with 90-μm-diameter, flat topped nozzles at 56 °C. The tapered nozzle process was performed on single nozzle devices, but it was designed to be compatible with multiplexed nozzle arrays. A dense array of tapered nozzles could meet a minimum power requirement, while using very low flow rates per nozzle to obtain small combustor geometries.

6. References

1. Waits, C. Thermophotovoltaic Energy Conversion for Personal Power Sources, 2012.
2. Deng, W.; Waits, C. M.; Morgan, B.; Gomez, A. Compact Multiplexing of Monodisperse Electrosprays. *Journal of Aerosol Science* **Oct 2009**, *40*, 907–918.
3. Waits, C. M.; Hanrahan, B.; Lee, I. Multiplexed Electrospray Scaling for Liquid Fuel Injection. *Journal of Micromechanics and Microengineering* **Oct 2010**, *20*.
4. Delamora, J. F.; Loscertales, I. G. The Current Emitted By Highly Conducting Taylor Cones. *Journal of Fluid Mechanics* **Feb 10, 1994**, *260*, 155–184.
5. Ganan-Calvo, A. M. Cone-jet Analytical Extension of Taylor's Electrostatic Solution and the Asymptotic Universal Scaling Laws in Electrospraying. *Physical Review Letters* **Jul 14, 1997**, *79*, 217–220.
6. Deng, W. W. Fundamentals and Applications of Multiplexed Electrosprays, Ph.D., Mechanical Engineering, Yale University, 2008.
7. Deng, W. W.; Gomez, A. Full Transient Response of Taylor Cones to a Step Change in Electric Field. *Microfluidics and Nanofluidics* **Jan 2012**, *12*, 383–393.
8. Krpoun, R.; Shea, H. R. A Method to Determine the Onset Voltage of Single and Arrays of Electrospray Emitters. *Journal of Applied Physics* **Sep 2008**, *104*.
9. Velasquez-Garcia, L. F.; Akinwande, A. I.; Martinez-Sanchez, M. A Micro-fabricated Linear Array of Electrospray Emitters for Thruster Applications. *Journal of Microelectromechanical Systems* **Oct 2006**, *15*, 1260–1271.
10. Deng, W.; Klemic, J. F.; Li, X.; Reed, M. A.; Gomez, A. Liquid Fuel Microcombustor Using Microfabricated Multiplexed Electrospray Sources. *Proceedings of the Combustion Institute*, vol. 31, pp. 2239–2246, 2007.
11. Williams, K. R.; Gupta, K.; Wasilik, M. Etch rates for Micromachining Processing - Part II. *Journal of Microelectromechanical Systems* **Dec 2003**, *12*, 761–778.

List of Symbols, Abbreviations, and Acronyms

DRIE	deep-reactive ion etch
E-spray	electro-spray
H_2O	water
H_2O_2	hydrogen peroxide
HCl	hydrogen chloride
HNA	hydrofluoric acid + nitric acid + acetic acid
ID	inner diameter
MES	multiplexed E-spray
NH_4OH	ammonium hydroxide
OD	outer diameter
SEM	scanning electron microscopy
Si_2N_3	silicon nitride
SiO_2	silicon dioxide
UAVs	unmanned aerial vehicles
WD	working distance

NO. OF COPIES	ORGANIZATION
1 ELEC	ADMNSTR DEFNS TECHL INFO CTR ATTN DTIC OCP 8725 JOHN J KINGMAN RD STE 0944 FT BELVOIR VA 22060-6218
7	US ARMY RSRCH LAB ATTN IMAL HRA MAIL & RECORDS MGMT ATTN RDRL CIO LL TECHL LIB ATTN RDRL CIO LT TECHL PUB ATTN RDRL SED E P BARNES B. HANRAHAN C MIKE WAITS RDRL VTP M KWEON